Targeting conformationally distinct amyloid polymorphs via symmetric de novo design

by
Hailey Wallace

DISSERTATION
Submitted in partial satisfaction of the requirements for degree of
DOCTOR OF PHILOSOPHY

in

Biophysics

in the

GRADUATE DIVISION
of the
UNIVERSITY OF CALIFORNIA, SAN FRANCISCO

Approved:

DocuSigned by:
William DeGrado
582727E949C7441...

William DeGrado
Chair

DocuSigned by:
David Agard

David Agard

DocuSigned by:
Tanja Kortemme

Tanja Kortemme

DocuSigned by:
Carlo Condello
3EA8184A6A7D419...

Carlo Condello

Committee Members

Targeting conformationally distinct amyloid polymorphs via symmetric de novo design

Hailey M. Wallace

Abstract

Amyloid formation, a hallmark of neurodegenerative disease and disorders, is associated with the self-assembly of amyloidogenic proteins into insoluble, beta-strand-rich fibrillar structures. The conformational heterogeneity of amyloids presents a significant challenge in developing effective therapeutic strategies. This study introduces novel computational methods to engineer a conformation-specific amyloid binder that identifies a single conformational strain of different amyloids formed from the same or closely related protein sequences. Thus, we identify surfaces unique to the conformational strain of interest, and repeating beta-strands become the “target backbone” for the design of a binder. Next, we identify structures in the PDB protein structure file with structures similar to the target based on backbone RMSD. We use clustering to identify neighboring structural motifs interacting with the backbone target of interest. This method identified monomeric helical motifs in favorable geometric arrangements for interaction with the amyloid. Each interacting helical motif was then replicated using the symmetry of the repeating amyloid structure, forming a helical sheet with geometric complementarity to the targeted region of the repeating beta-sheet. In the complexes, each helix interacts with two beta strands and two neighboring helices. Sequences were next designed for structures with favorable helix-helix and helix-sheet geometries, keeping the native sequence constant and applying symmetrical restraints on the helical monomers. We used this computational pipeline to design peptides that bind to a conformational form of a-synuclein fibrils with high specificity relative to other amyloids formed by a-synuclein, tau, or Abeta40. Fluorescence microscopy and bulk binding assays showed that one of the designed peptides indeed bound with high specificity to a-synuclein, and aggregation assays showed that it markedly retarded its rate of amyloid formation. These novel

methods offer new tools for examining conformational strains of amyloid proteins and pave the way for developing personalized therapies tailored to specific amyloid-related diseases.

Table of Contents

Introduction 1

Results 5

Computational Design Pipeline 5

Biophysical characterization of peptides 12

Discussion 21

Materials and Methods. 24

Fibrillization 24

Solid-phase peptide synthesis of amyloid-binding peptides 24

Ligand depletion sedimentation assay 25

Confocal microscopy 26

References 28

List of Figures

Figure 1. Amyloid fibril formation pathway 2

Figure 2. Amyloid polymorphism 3

Figure 3. Computational search for starting scaffolds using Q-BITS and MASTER 7

Figure 4. Computational overview using Q-BITS output 8

Figure. 5. Symmetry application and interaction energy 9

Figure 6. Interaction energies vs. packing scores of designed peptides to amyloid 11

Figure 7. Confocal images of synthesized peptides with α-synuclein RT 14

Figure 8. Confocal images of Pep-AAKS overlayed with ThT control on α-synuclein RT 14

Figure 9. Confocal images of Pep-AAKS with amyloid beta 40, tau, and α-synuclein RT 15

Figure 10. Confocal images of Pep-AAKS with controls 15

Figure 11. Thermal denaturation, mass spectrometry analysis, and circular dichroism data of Pep-AAKS 16

Figure 12. Ligand depletion sedimentation assay 18

Figure 13. Binding curve from ligand depletion sedimentation assay 18

Figure 14. Fibrillization kinetics of α-synuclein RT with and without the presence of Pep-AAKS 20

Figure 15. Putative inhibition method of Pep-AAKS 20

List of Tables

Table 1. Table of peptide sequences that were synthesized and tested for binding to α-synuclein 13

List of Abbreviations

Cell-Penetrating Peptides (CPP) **4**

Cryo-electron microscopy (cryo-EM) **1**

Fluorescein-5-isothiocyanate (FITC) **12**

Nuclear magnetic spectroscopy (NMR) **1**

Sulforhodamine 101 acid chloride (Texas Red) **12**

Surface plasmon resonance (SPR) **1**

Thioflavin T (ThT) **12**

Introduction

Amyloids have emerged as a hallmark in the pathogenesis of neurodegenerative and many non-neurodegenerative diseases. The formation of amyloid fibrils occurs through the self-assembly of amyloidogenic proteins. These amyloidogenic proteins aggregate after aberrant conformational changes and misfolding, resulting in an accumulation of beta-strand-rich, insoluble fibrils, as shown in Figure. 1. The misfolded monomers in the fibrils are stacked against one another and interdigitate as beta sheets through steric zipper interactions.[1,2] These amyloid structures have been linked to a diverse range of disorders – from incurable neurodegenerative diseases like Alzheimer's and Parkinson's disease to type 2 diabetes, making them a focal point of scientific investigation. In particular, alpha-synuclein misfolding is associated with the accumulation of toxic oligomers and fibrils found in intracellular Lewy bodies in the neurons of patients with Parkinson's disease.[3] These amyloid aggregates have been shown to induce cellular dysfunction, neuronal damage, and neuroinflammation, leading to the progressive loss of cognitive and motor functions.[4,5] Current biophysical characterization of these amyloid aggregates is able to shed light on amyloid structural properties, stability, and assembly pathways through means such as cryo-electron microscopy (cryo-EM)[1], nuclear magnetic spectroscopy (NMR)[6,7], and surface plasmon resonance (SPR)[8].

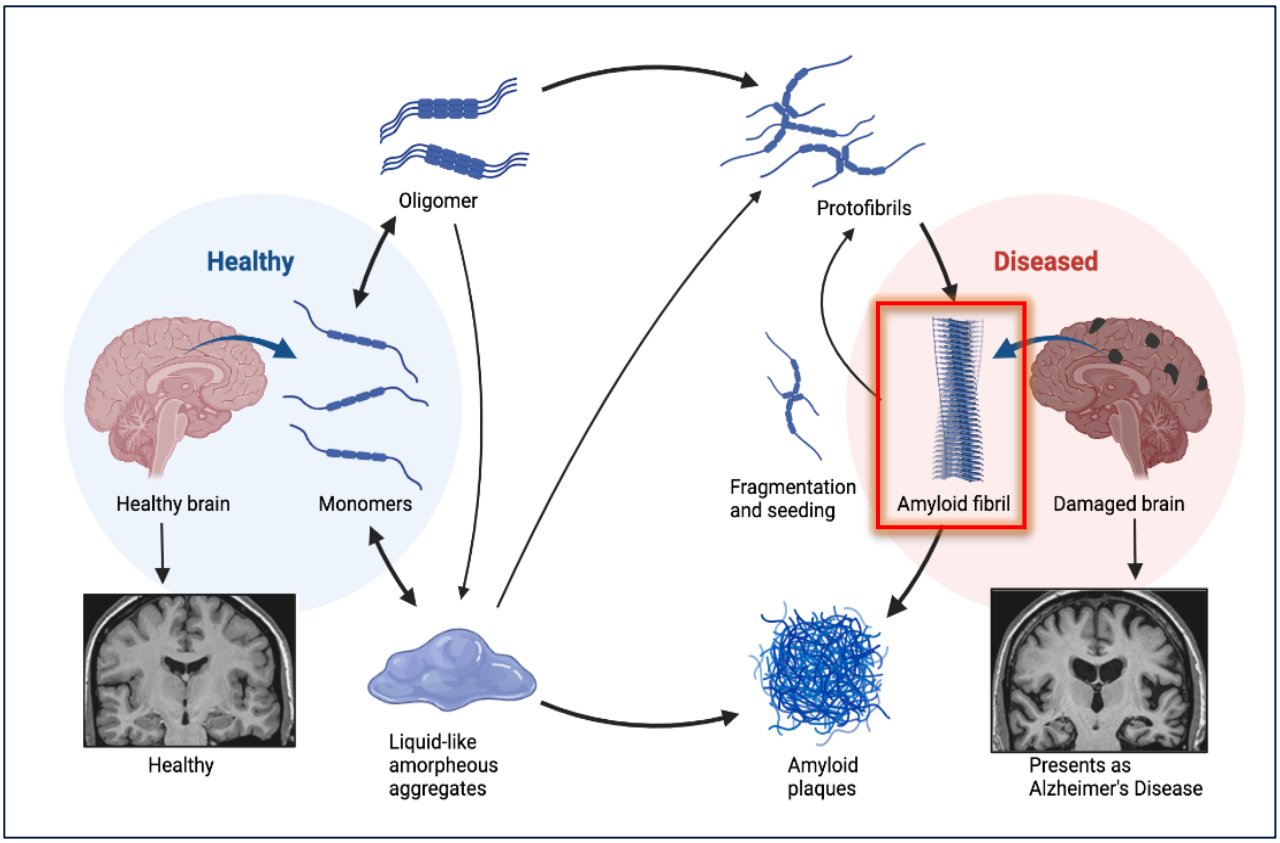

Figure 1. Amyloid fibril formation pathway. Amyloid formation pathway results in many amyloid conformational polymorphs. The amyloid formation pathway illustrates how a monomeric protein misfolds and self-assembles into a highly ordered amyloid (red box).

The complexity of amyloid-related disorders is further compounded by the distinct conformations (conformational strains) that amyloids can adopt, which vary with the disease type and, in some cases, are heterogeneous within a single brain.[9,10] For instance, alpha-synuclein can form multiple conformations of amyloid, termed polymorphs, with varying degrees of toxicity.[11] Examples of amyloid polymorphism are displayed in Figure 2. This adds a layer of intricacy to the amyloid disease pathophysiology as well as to our current understanding of protein biophysics.

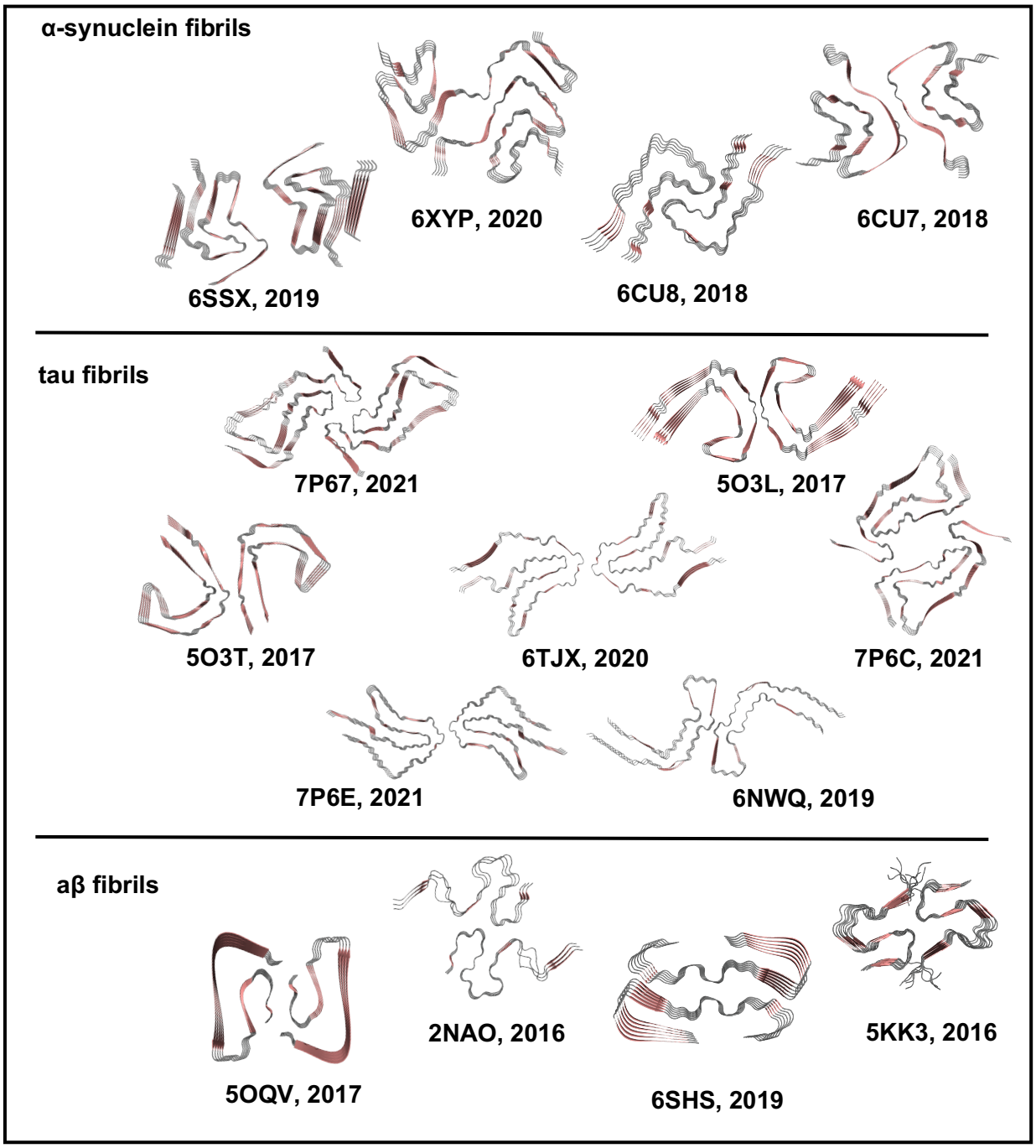

Figure 2. Amyloid polymorphism. Examples of different amyloid conformations, or polymorphs, arising from α-synuclein, tau, or aβ protein.

Considerable research efforts in amyloid biophysics and amyloid formation have focused on designing molecules that can interact and inhibit amyloid formation. Current approaches to understanding the biophysical principles underlying amyloid inhibition have utilized small molecules, peptides, and antibodies as a tool to disrupt this aggregation process.[12–20] Peptide-based inhibitors have gained popularity due to their advantages in specificity, biocompatibility, and potential for therapeutic delivery. Designed Cell-Penetrating Peptides (CPP) have demonstrated the ability to inhibit Aβ aggregation and cytotoxicity.[20] Progress has also been made in the field of protein design to engineer high-affinity amyloid capping peptides that inhibit amyloid growth.[14,18,19] Recently, amyloidogenic peptide traps have been rationally designed to sequester monomeric proteins before their initial aggregation, preventing the formation of amyloid fibrils.[21]

However, the diverse conformational landscape of amyloids presents a considerable challenge in developing effective therapeutic strategies for neurodegenerative diseases. Conformational differences in amyloids have been linked to distinct modes of assembly and degrees of toxicity.[5] To broaden our understanding of amyloid formation and the link between amyloid conformation and cytotoxicity, it is essential to create binders specific to distinct conformational strains. Historically, the only methods that have been available to researchers to parse out conformational differences amongst amyloid polymorphs have been expensive and time-consuming structure determination methods like cryo-EM. Additionally, experimental screening has identified fluorescent dyes that identify distinct conformational forms, but their mode of conformational discrimination is not known. Examples of these include EMBER which parses conformational differences in amyloid-β and tau deposits[22] and oligothiophene dyes which differentiate PrP strains[23], amyloid-β, and α-synuclein strains.[24]

In this work, we develop computational methods to design peptides that bind amyloids in both sequence and structure-specific manners. The strain-specific binders will provide novel tools for investigating the link between amyloid conformation and toxicity. Furthermore, by interacting with unique structural motifs within amyloid polymorphs, these peptides disrupt aggregation pathways, which may provide an avenue for therapeutic development in mitigating amyloid toxicity. Finally, our computational approach should allow for new tools for the structure-based design of proteins that bind to any protein surface.

Results

Computational Design Pipeline

The binding region of the amyloid of interest was designated by searching for exposed epitopes that are solvent accessible in one polymorph and not in another. We chose the Rod polymorph from α-synuclein RT as our initial test model.[25] At the time of the initiation of this work, structures were also available for tens of additional forms of native or familial mutants of a-synuclein. Additionally, the α-synuclein RT fibrils are also formed recombinantly without using cofactors, like with tau, which is why the Rod polymorph from α-synuclein RT was our initial test model. We first identified distinguishable regions that differed in solvent-accessible surface area and were able to accommodate the binding of a designed peptide to the surface of the amyloid. Amyloid structures were acquired through AmyPro[26] and solvent-accessible surface area calculations were done with FreeSASA.[27] These distinguishable regions are stacked along the z-axis of the amyloid, allowing us to use a translational symmetry that coincides with the symmetry of the amyloid. Thus, we can identify repeat peptides that cooperatively bind across the fibril's surface.

Representatives from the clustered output from the initial MASTER search were filtered for alpha helices. Alpha helices are less prone to aggregation and amyloid formation, so this secondary structure was desirable for a binder. We furthermore sought starting motifs that were found to run near parallel to the amyloid so that the translational symmetry across the z-axis of the fibril may be accommodated by the binder. The filtered output of secondary structures that match these criteria was then aligned across the extended fibril axis so that the peptide to amyloid stoichiometry was 1:2. This method is displayed in Figure 3. The interval between beta sheets of an amyloid is roughly 4.8 Angstroms. The interval between our peptide backbones averages 9.9 Angstroms, which is the middle distribution for helix-helix packing in natural proteins. We sought to confirm our stacked peptide is still represented by natural proteins. To do this, we scanned the MASTER[28] database for 10-residue fragments from two chains of our aligned helices for matches in the PDB that are under 1.0 Angstrom Cα RMSD, as shown in Figure 4. If there were at least one hundred matching fragments in the PDB for our designed helix-helix interaction, then we deemed it as a “designable” scaffold-scaffold interface. About ninety percent of scaffolds fit these criteria, with some scaffolds having thousands of matches.

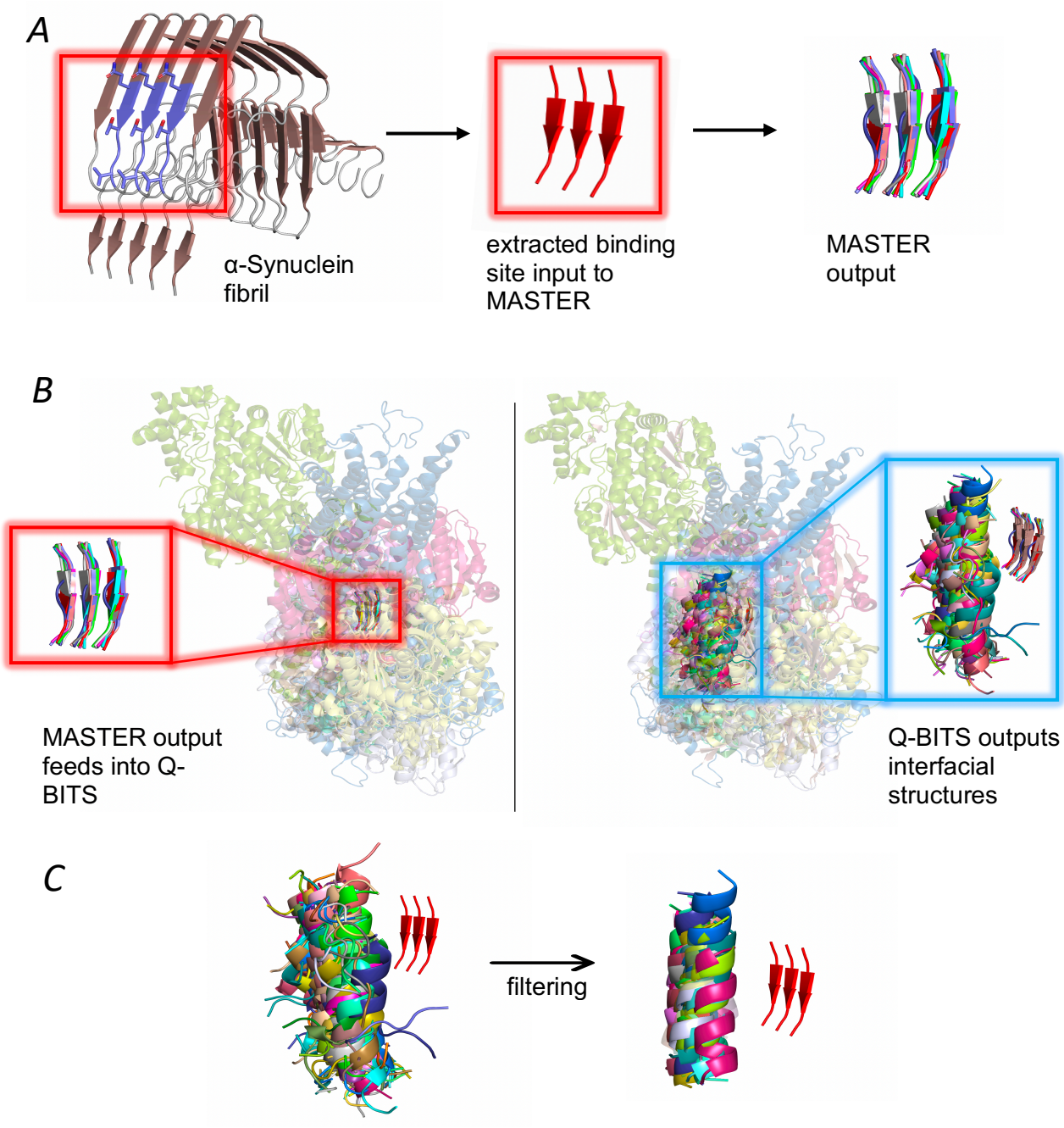

Figure 3. Computational search for starting scaffolds using Q-BITS and MASTER. A. The binding site is extracted from the starting PDB and then input into MASTER. MASTER outputs low RMSD fragments from known PDB structures. B. This MASTER output is fed into Q-BITS to find scaffolds that compliment that binding site from the parent PDBs of the MASTER output. C. These Q-BITS complimentary scaffolds are filtered for helical secondary structure.

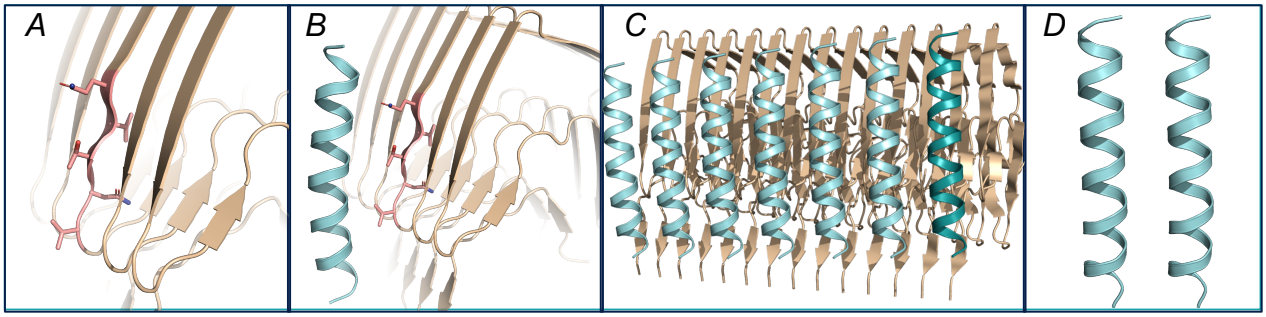

Figure 4. Computational overview using Q-BITS output. Amyloid is shown in tan. A. The solvent-exposed distinguishable region where a peptide will target is shown in salmon. B. Searching for scaffolds via Q-BITS for design produces helices (cyan) at the distinguishable region. C. The final peptides have symmetry that matches the natural amyloid's twist. D. Helix-helix interactions are cross-checked with the program MASTER to confirm interhelical designability.

After filtering and aligning the peptide scaffolds, we generated symmetry files using the Rosetta software.[29,30] These symmetry files were crucial in defining the helical translation of the peptide along the amyloid axis. An independent symmetry file was created for each of the 75 peptide scaffolds complexed with the amyloid, containing detailed information on the rotation between subunits, the translation or pitch, and the distance between subunits. These parameters were carefully curated to match the cryo-EM model of the amyloid, where each symmetry subunit corresponds to 1 peptide backbone to 2 amyloid beta strands, as shown in Figure 5. The symmetry files were pivotal in enabling structural and sequential peptide repeats, allowing the amyloid-peptide complex to propagate.

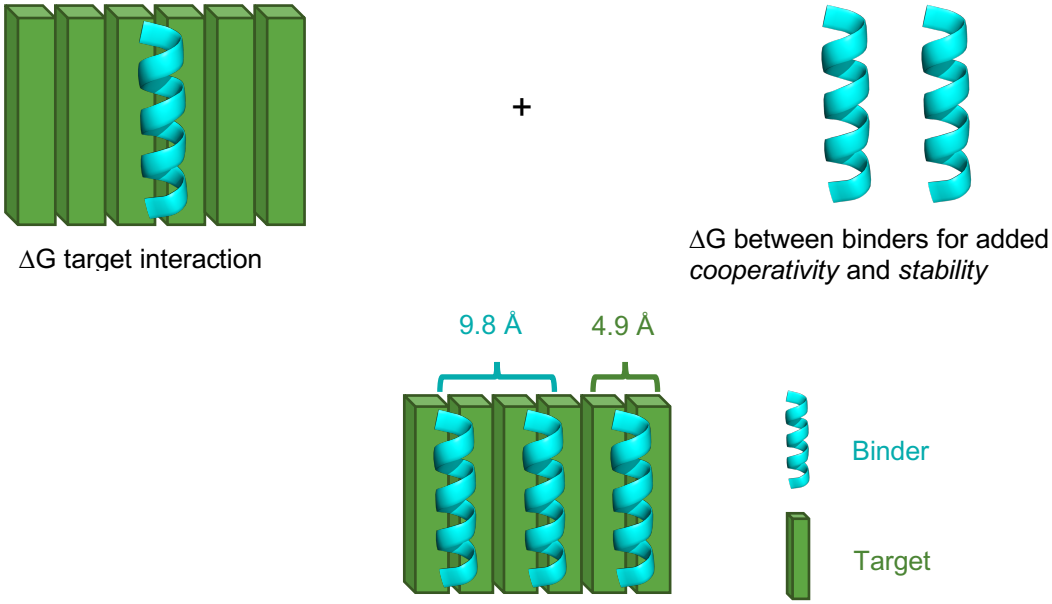

Figure 5. Symmetry application and interaction energy. Perfect symmetry of the peptide matching the natural amyloid is essential for this peptide-amyloid geometry to propagate along the fibril axis.

To facilitate the design process, we also generated residue files, commonly known as resfiles, which focused on fixing the amyloid while sampling rotamers exclusively on the peptide binder scaffold. With the help of Rosetta's HBNet and each peptide's symmetry file, we conducted an extensive search to identify potential hydrogen bonding residues at the interface of both the amyloid-peptide and peptide-peptide repeats.[31] These hydrogen-bonded residues were constrained, and we proceeded with a flexible backbone design using Rosetta. Each peptide scaffold was subjected to design simulations to produce 1,000 models, resulting in a total of 75,000 designs. Detailed scripts used for these design runs can be found in the supplementary materials.

Designs were chosen based on their residue packing at the interface, assessed using Rosetta's pstat score. Additionally, a combination of interaction energies, employing ref2015 weights, was considered from a pool of 75,000 designs derived from 75 different peptide backbones. The interaction energies were calculated by comparing the overall energy between a single peptide complexed with six beta strands (peptide and amyloid interaction), the individual peptide, and the six beta strands. This energy difference was further supplemented with the energy variation between two interacting peptides and two individual peptides. This interaction energy served as a useful measure for evaluating amyloid binding energy and positive cooperativity between peptides. A plot of this packing score vs. interaction energy of for one of the scaffolds is shown in Figure 6. During the selection process, designs were filtered to exclude those with any buried unsatisfied hydrogen bonds, ensuring only the most promising candidates were retained for further investigation.

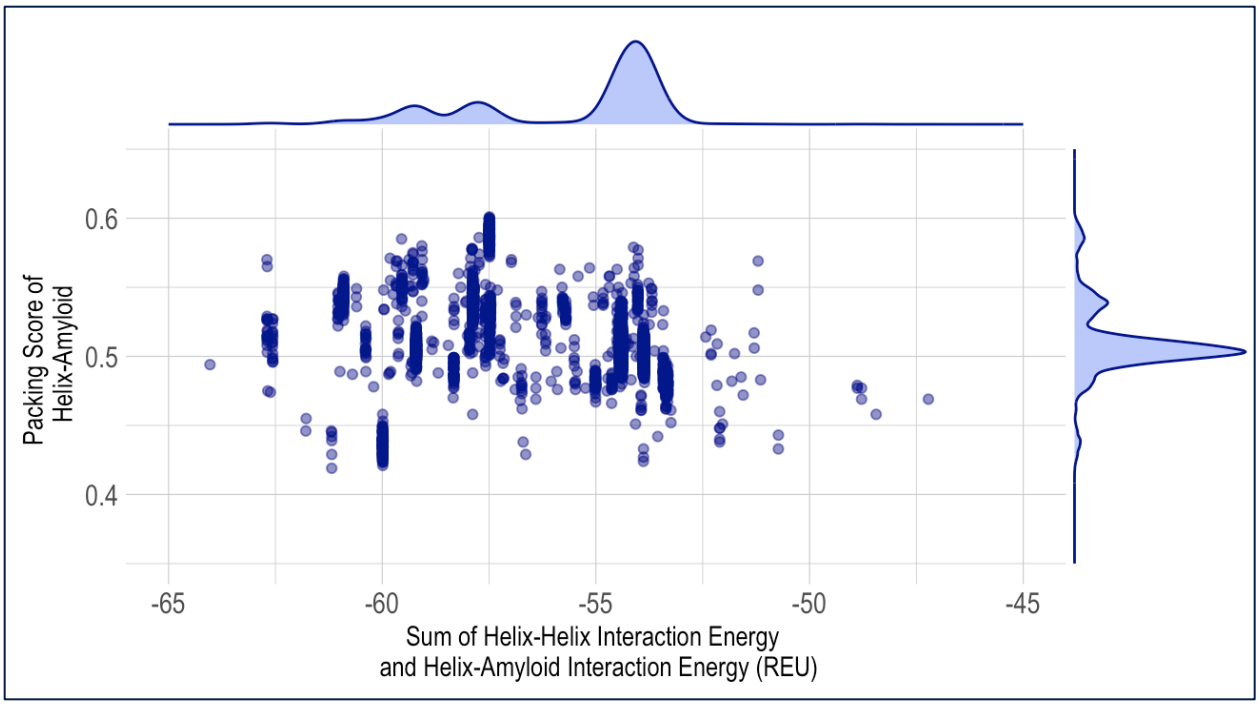

Figure 6. Interaction energies vs. packing scores of designed peptides to amyloid. Each point represents a different design model with plotted distributions on the x and y-axis. Each design model's interaction energy is plotted against the packing score. Red box indicates the experimentally tested peptide sequences.

Biophysical characterization of peptides

From the top-scoring peptide binder sequences, we selected 8 for the first round of experimental testing. Amyloid-binding peptides were successfully synthesized using a Biotage Initiator+ Alstra peptide synthesizer on a 0.05 mmol scale, following standard peptide synthesis protocols. Fluorescein-5-isothiocyanate (FITC) and sulforhodamine 101 acid chloride (Texas red) were conjugated to the N-termini of the peptides on resin, with the confirmation of successful dye conjugation achieved through mass spectrometry and analytical HPLC. Confocal microscopy was used to visualize the fibril-peptide complexes.

We successfully reconstituted α-synuclein monomers in the fibrillization solution containing 15 mM tetrabutylphosphonium bromide, achieving a final concentration of 300 μM as per Eisenberg's fibrilization protocol.[25] Over a seven-day period, fibrils were grown from these α-synuclein monomers with continuous shaking at at 37 °C, using either a 384-well plate or 1 mL non-stick Eppendorf tubes. Complete fibrillization was validated using the FLUOstar OMEGA Microplate Reader, and thioflavin T (ThT) fluorescence confirmed the presence of beta-strand-rich fibrils.

Peptides were prepared at different concentrations (ranging from 1 nM to 128 nM) and mixed with fully formed α-synuclein fibrils at a final fibril concentration of 600 nM. Recombinant E46K α-synuclein fibrils[32], amyloid beta, and tau fibrils were used as a control. Confocal imaging revealed interactions between the peptides and amyloid fibrils, offering a valuable perspective on their binding affinity and behavior (Figures 7, 8, 9, 10). One peptide (PepAAKS) displayed better binding than the other 7 peptides and was submitted to a second iteration of computational design. Following this second set of design, 7 more sequences were selected for synthesis and

experimental testing. These sequences are listed in Table 1. Confocal microscopy revealed that PepAAKS was indeed the best binder following both rounds of experimental testing and design. Thermal denaturation, mass spectrometry analysis, and circular dichroism data of Pep-AAKS are shown in Figure 11.

Table 1. Table of peptide sequences that were synthesized and tested for binding to α-synuclein.

Design round	Model name	Sequence	MW with ALA/FITC (Da)
1	monomer_384	KMWELWARMAKEAFKMAESAAKS	3161.22
1	monomer_14res_2res_181	SMLEEVVKAGREIIAS	2192.03
1	543_842_0019	SWEEIIKALAELMRKVLEALSKL	3131.23
1	monomer_14res_2res_181_mut_Thr	SMLEETVKAGREIIAS	2194.00
1	14res_2res_761_0008	SMLEKVVEAGQKIVAK	2190.10
1	384_576_003	KMWELWARMAKEAFKMAESAYKS	3253.31
2	scrambled_1sequence	ASKAKMAAEKRWMESLWEAMKAF	3161.22
2	helical_control	SEEEKRKSDAERRRREKEWNSKK	3422.24
2	Best_flex_3139	RMWELWADMAKKAFDMATEAAKT	3162.18
2	flex_4306	KMWELWARMAKWAFEMAAEAAKT	3217.30
2	best_fix_186	KMWELWARMAKEAFKMADSAAKT	3161.22
2	fix_641	KMWELWARMAKWAFEMADSAAKT	3219.27
2	fix_246	KMWELWARMAKEAFKMAREAAKT	3244.37

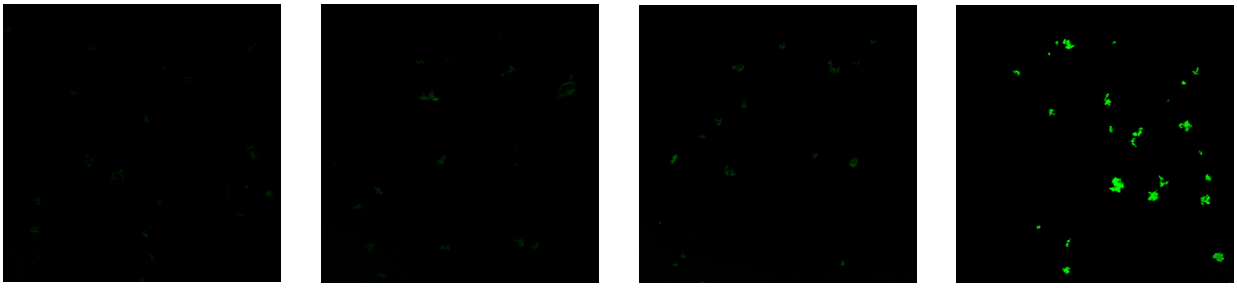

Peptide 543_842_0019 | Peptide 14res_2res_761_0008 | Peptide 384_576_003 | Pep-AAKS (monomer_384)

Figure 7. Confocal images of synthesized peptides with α-synuclein RT. 10nM synthesized peptides conjugated to FITC on 100ng/mL α-synuclein RT. Excitation/emission is 490/515 nm. Pep-AAKS (right) shows intense puncta indicative of peptide localization to amyloid.

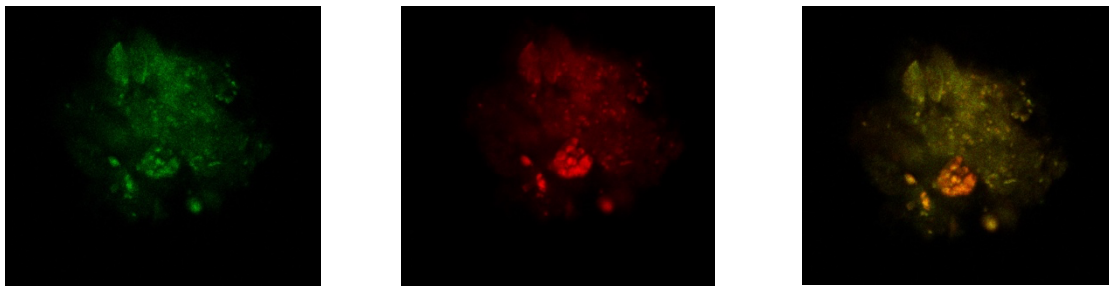

440/490nm ex/em | 561/594nm ex/em | Overlay: 440/490nm and 561/594nm ex/em

Figure 8. Confocal images of Pep-AAKS overlayed with ThT control on α-synuclein RT. 10nM synthesized peptides conjugated to Texas Red on 100ng/mL α-synuclein RT. Texas Red dye was used due to having no spectral overlap with ThT. The left image shows the excitation/emission capturing ThT, a known amyloid binder, indicating the presence of amyloid fibrils. The middle image shows the excitation/emission capturing Texas Red dye that is conjugated to peptide. The right image shows and overlap of these spectra, indicating that the peptide localizes to amyloid.

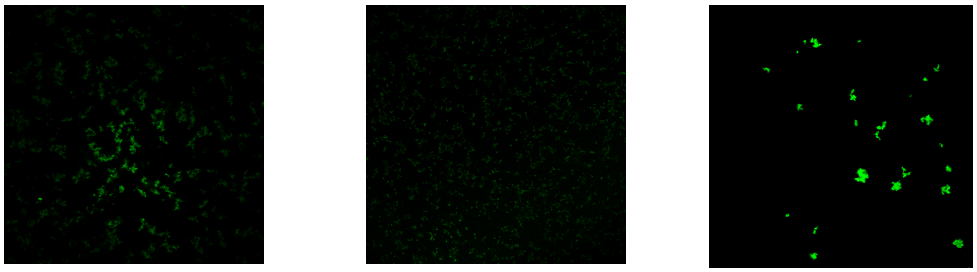

Figure 9. Confocal images of Pep-AAKS with amyloid beta 40, tau, and α-synuclein RT. 10nM Pep-AAKS conjugated to FITC on 100ng/mL amyloid beta 40, tau, and α-synuclein RT. Excitation/emission is 490/515 nm. Pep-AAKS on α-synuclein RT (right) shows significantly more intense puncta than on other amyloids indicative of specificity to α-synuclein RT.

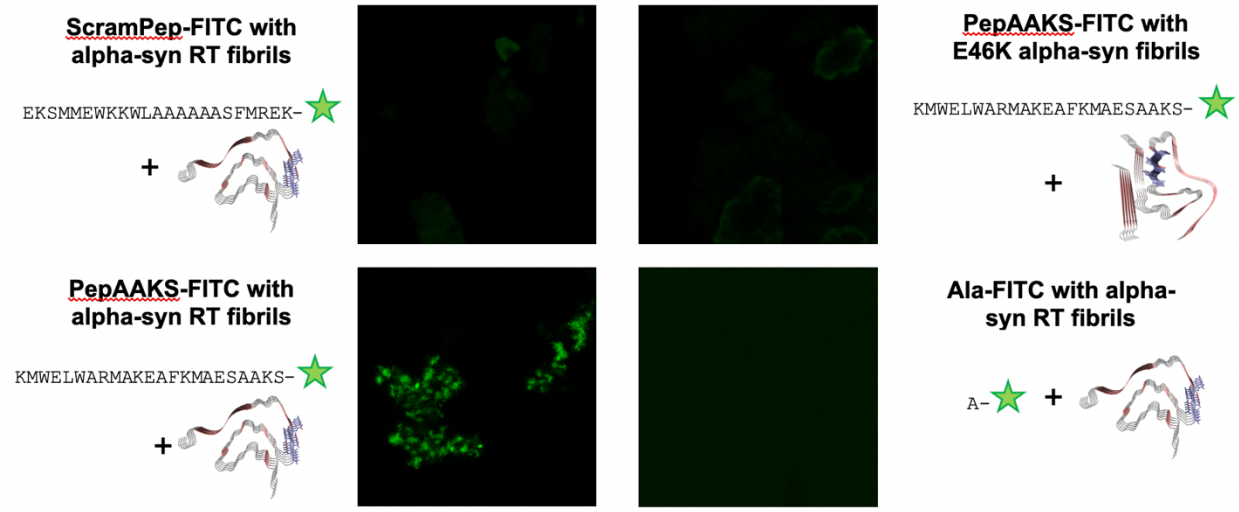

Figure 10. Confocal images of Pep-AAKS with controls. Confocal images of 600nM amyloid with 258nM fluorescently tagged peptide samples. Top left – scrambled peptide control with α-Synuclein RT (control). Top right – PepAAKS with α-Synuclein E46K (control). Bottom right – monopeptide with α-Synuclein RT (control). Bottom left – PepAAKS with α-Synuclein RT.

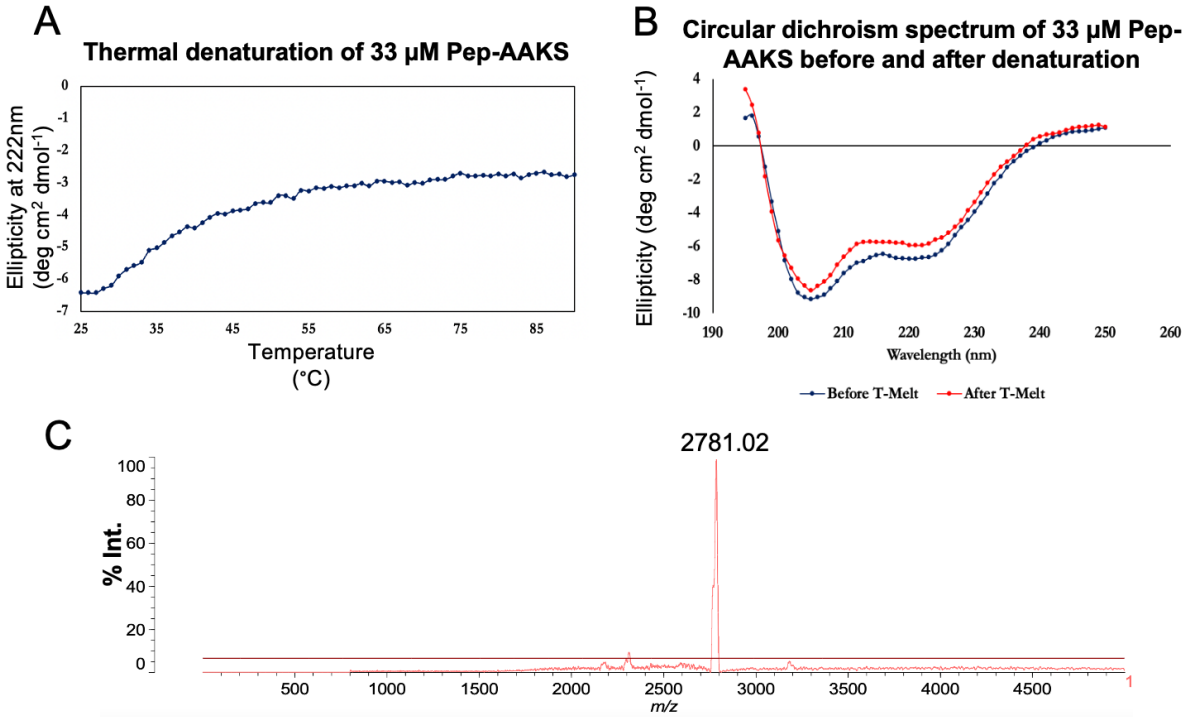

Figure 11. Thermal denaturation, mass spectrometry analysis, and circular dichroism data of Pep-AAKS. A. Thermal denaturation of Pep-AAKS. Curve shows melting at 45 ℃ at 33 µM of Pep-AAKS, indicative of peptides. B. Circular dichroism spectrum of Pep-AAKS. Curve shows helical secondary structure of Pep-AAKS at 33 µM. C. MALDI of PepAAKS-FITC. Expected mass is 2772 Da.

The interaction between Pep-AAKS and α-synuclein fibrils was investigated using ligand depletion sedimentation assays, outlined in Figure 12. Fibril-peptide solutions were prepared at a final peptide concentration of 9.5 μM and varying α-synuclein fibril concentrations ranging from 5 to 40 μM. A scrambled peptide sequence and E46K α-synuclein fibrils were used as a control. The following quadratic binding formula using a stoichiometry of two beta strands to one peptide was used:

$$\frac{[PL]}{[P]_T} = \frac{\left(K_D + \frac{[P]_T}{2} + [L]_T \pm \sqrt{\left(K_D + \frac{[P]_T}{2} + [L]_T\right)^2 - \frac{4[P]_T[L]_T}{2}]}\right)}{\frac{2[P]_T}{2}}$$

Fitting these data to the previous equation, the apparent dissociation constant of Pep-AAKS to α-synuclein RT was 2.29 μM, plotted in Figure 13.

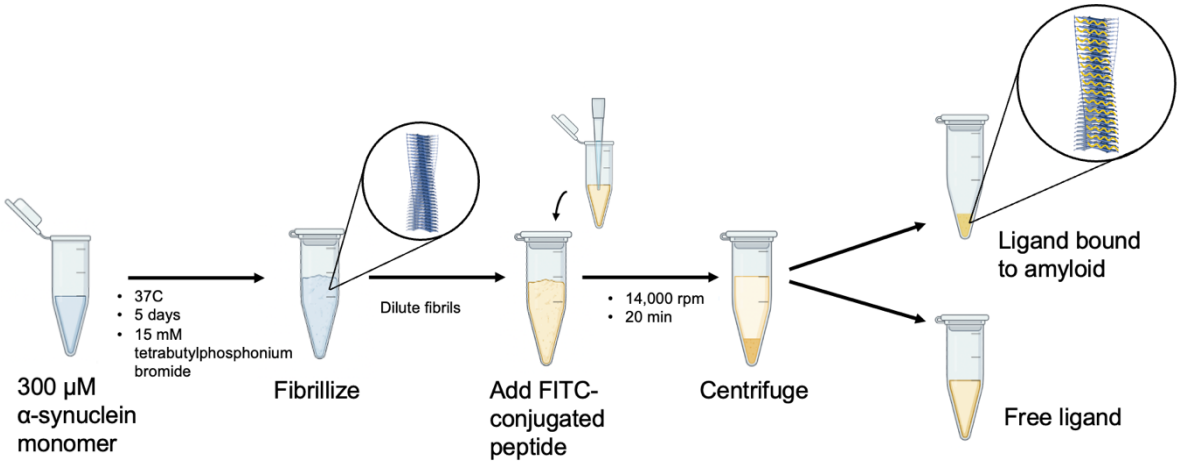

Figure 12. Ligand depletion sedimentation assay. Initial α-synuclein monomer is fibrillized according to Eisenberg's fibrillization protocol.[25] Labeled peptide is added to the formed fibril and centrifuged. The depleted ligand in the supernatant is quantified and the peptide-amyloid complex in the pellet is calculated.

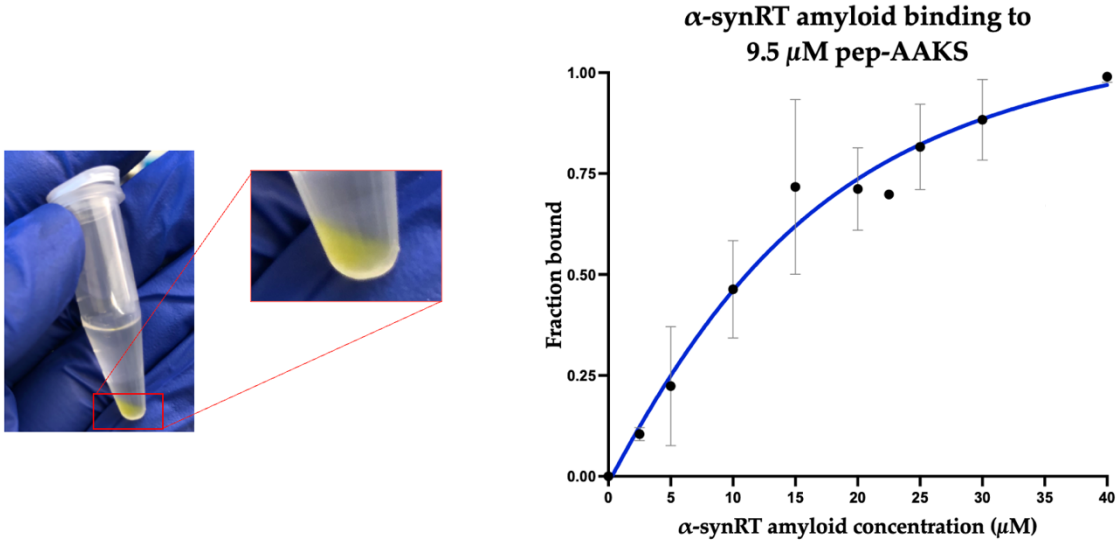

Figure 13. Binding curve from ligand depletion sedimentation assay. Left image shows the sedimented peptide labeled with FITC complexed with amyloid. Right image shows these data and apparent dissociation constant.

We then recorded the fibrillization kinetics of α-synuclein RT with and without the presence of Pep-AAKS using Eisenberg's fibrilization protocol.[25] 200 μM of Pep-AAKS was combined with the 300 μM α-synuclein monomer in the fibrillization solution and shaken at 37 °C with 6 μM ThT. Nine replicates for each condition were created. Pep-AAKS with ThT was used as a control and showed no signal increase over time, indicating there was no fibril formation amongst the peptides by themselves. The α-synuclein samples that included Pep-AAKS showed retardation of fibril formation, indicated by the lag of fluorescence signal increase (Figure 14). This inhibition of fibril formation may be due to the peptide blocking secondary nucleation (Figure 15). If so, this would open the door to new therapeutic approaches to treating amyloid-related diseases.

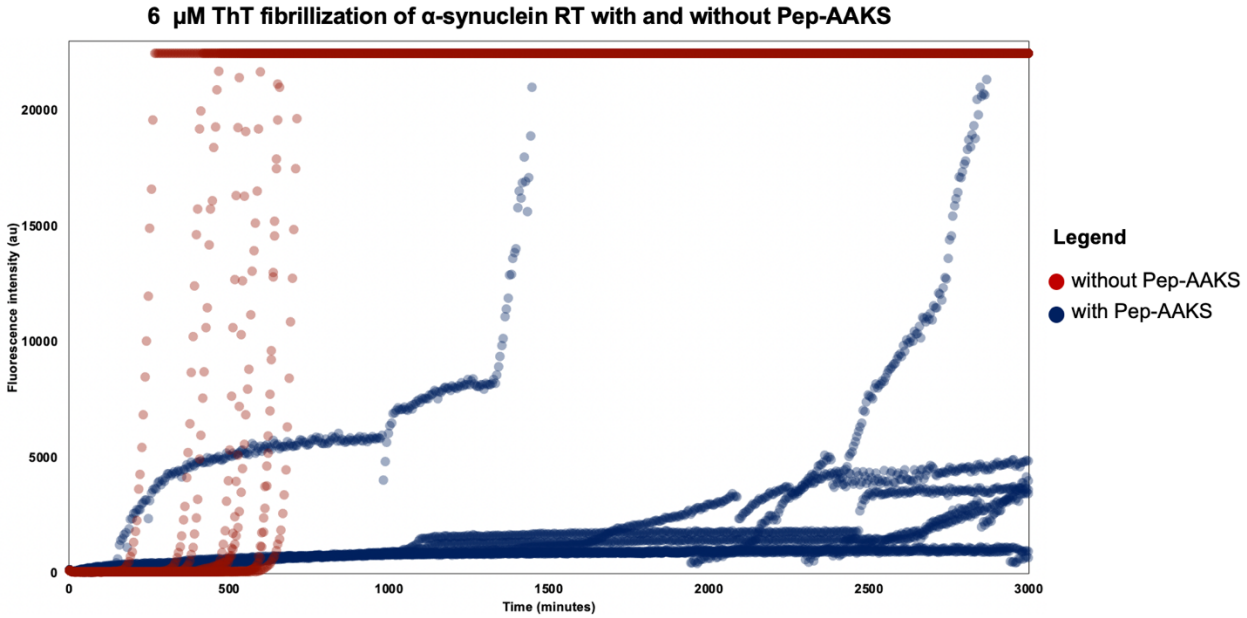

Figure 14. Fibrillization kinetics of α-synuclein RT with and without the presence of Pep-AAKS. Nine replicates α-synuclein with and without Pep-AAKS. All nine samples of α-synuclein with Pep-AAKS (blue) show a lag in fibril formation.

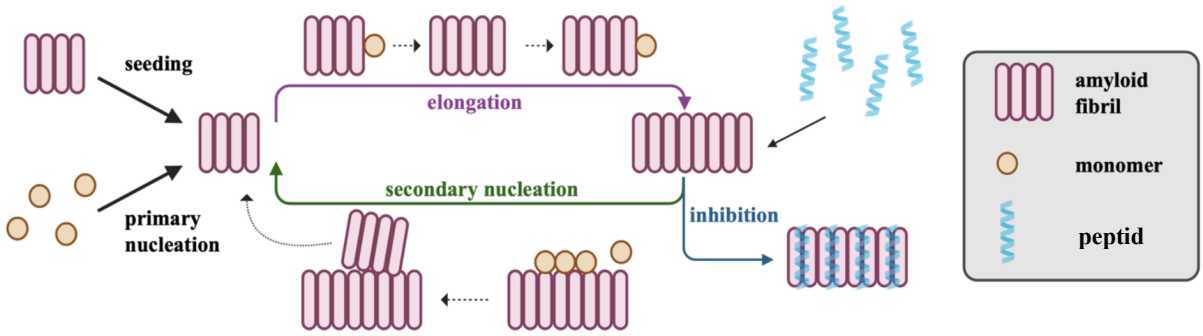

Figure 15. Putative inhibition method of Pep-AAKS. The putative mechanism of the amyloid-binding peptide inhibiting secondary nucleation of amyloid propagation.

Discussion

Amyloids are a hallmark in the pathogenesis of neurodegenerative disease. Amyloid formation is a result of the self-assembly of amyloidogenic proteins, leading to the formation of stacked, insoluble beta-strand-rich monomers. These conformationally distinct monomers interdigitate through steric zippers to form fibrillar, beta-sheet structures. These amyloid structures are closely associated with a wide range of disorders and diseases, highlighting the importance of understanding their biophysical properties so that we can progress the exploration of therapeutic intervention.

Our study focuses on developing new methods for exploring the conformational diversity of amyloids by designing novel peptides that can selectively bind to distinct amyloid polymorphs. These conformation-specific peptide binders will offer insight into the link between amyloid conformation and toxicity, thus providing new approaches to controlling the amyloid formation pathway in amyloid-related disorders and advancing therapeutic development.

In our computational design pipeline, we employed a rational approach to identify specific regions of amyloid surfaces that are distinguishable between polymorphs. These distinguishable regions, strands of amino acids with varying degrees of solvent-accessible surface area between conformations, serve as potential binding sites for de novo designed peptides. Leveraging translational symmetry design techniques within Rosetta, we identified repeat peptides capable of cooperatively binding across the fibril's surface.

To facilitate the peptide evaluation process, we performed extensive filtering and alignment of peptide scaffolds that were found with our novel computational program. Using alpha helices as starting motifs offered favorable stability for potential peptide binders. Moreover, the translational symmetry along the fibril axis was considered to allow for cooperative binding between peptides against the fibril surface with a design stoichiometry set at one peptide to two beta strands. Importantly, we verified that the designed stacked peptide backbones were similar to natural proteins, confirming the feasibility of our approach.

Through Rosetta, we generated symmetry files to precisely define the helical translational of peptides along the amyloid axis. These symmetry files contain crucial information regarding the rotation, translation, and distance between peptide subunits so that they perfectly match the symmetry of the original cryo-EM model of the amyloid target. This peptide symmetry that matches that of the amyloid target is essential for the propagating the amyloid-peptide complex.

Sequence design consisted of residue files that fix the amyloid backbone and rotamers while allowing rotamers on the peptide to be sampled. Rosetta's HBNet was used to search for potential hydrogen bonding residues at the interfaces of both the peptide-peptide and peptide-amyloid. These identified hydrogen-bonded residues were then constrained while a flexible backbone design algorithm in Rosetta was used to sequence design the rest of the peptide binder. This design process yielded a vast pool of roughly 75,000 designs derived from 75 different starting peptide scaffolds.

Design selection was based on the packing and the interaction energy between peptide-peptide and peptide-amyloid. This was performed using Rosetta's pstat score and a combination

of computationally derived interaction energies which served as a proxy for the amyloid binding and potential for peptide cooperative binding. Designs with any buried unsatisfied hydrogen bonds were also filtered out, ensuring the retention of only the most promising candidates.

Two rounds of such design were performed, and eight peptides from each round were selected from the top sequence candidates for synthesis. We successfully synthesized these peptides with fluorescent dyes on the N-termini for visualization under a confocal microscope. Our top peptide candidate, Pep-AAKS, was further analyzed via a ligand depletion sedimentation assay to derive an apparent dissociation constant. This apparent K_d of PepAAKS is 2.29 μM in the α-synuclein RT mixture.

In conclusion, our work represents a new method for engineering tools to elucidate the connection between the conformational diversity of amyloid and disease pathogenesis, thus opening the door to new therapeutic strategies for amyloid-related diseases. Furthermore, our computational approaches will allow for new de novo design techniques within the community. In this work, we highlight novel computational tools that can quickly parse from the PDB designable peptide scaffolds that can bind to any input protein. Moreover, our computational approach provides valuable tools for the identification of conformation-specific binding sites within protein homologs. The potential for personalized therapies tailored to specific amyloidopathies makes this research highly relevant in the field of amyloid biophysics and emerging therapeutic technologies.

Materials and Methods

Fibrillization

The lyophilized α-synuclein monomers were reconstituted in the fibrillization solution containing 15 mM tetrabutylphosphonium bromide, achieving a final α-synuclein concentration of 300 μM. Fibrils were grown from these α-synuclein monomers over a seven-day period, with continuous shaking at at 37 °C, employing either a 384-well plate (Corning™ BioCoat™ 384-Well, Collagen Type I-Treated, Flat-Bottom Microplate) or 1 mL non-stick Eppendorf tubes, as previously described.[25] Complete fibrillization was validated using the FLUOstar OMEGA Microplate Reader. Prior to fibrillization, the 50 μL α-synuclein monomer samples in the 384-well plate were combined with thioflavin T (ThT) to achieve a final concentration of 15 μM ThT per sample well. ThT, known for its affinity to beta sheets in amyloids, served as an indicator for beta-strand-rich fibril formation.[33] Emission data were collected during the fibrillization process to monitor beta-strand formation over time, which is indicative of fibril formation. The samples were excited at 440 nm, and the emission data were measured at 490 nm every 10 minutes throughout the seven-day fibrillization period. The 384-well plate was shaken for 5 minutes before data collection, and it remained stationary during data acquisition. Once α-synuclein fibrillization was confirmed, the same protocol was scaled up to 100 μL of α-synuclein monomer and fibrillization solution in the 1 mL non-stick Eppendorf tubes.

Solid-phase peptide synthesis of amyloid-binding peptides

The peptides were synthesized using a Biotage Initiator+ Alstra peptide synthesizer on a 0.05 mmol scale, following standard peptide synthesis protocols. Fmoc deprotection, washing, and double coupling reaction cycles were employed during the synthesis. Deprotection was

accomplished by treating the resin-bound peptides with 4.5 mL of 20% 4-methylpiperidine in DMF at 70 ºC for 5 minutes. Double coupling involved sequential coupling of each Fmoc-protected amino acid in the presence of 5 equivalents of Fmoc-protected amino acids, 5 equivalents of HCTU relative to the peptide functional sites, and 10 equivalents of DIPEA in DMF relative to the peptide functional sites, at 75 ºC for 5 minutes.

For the tagged peptides, fluorescent dyes, namely fluorescein-5-isothiocyanate (FITC) and sulforhodamine 101 acid chloride (Texas red), were conjugated to the N-termini of the peptides on resin. Each dye was added to the peptide on resin at 2.5 equivalents along with 5 equivalents of DIPEA relative to the peptide functional sites. The mixture containing the peptide on resin, DIPEA, and dye was allowed to react at room temperature for 5 hours under aluminum foil. Subsequently, the resin was washed with 3 rinses of DMF and 4 rinses of DCM before being dried for 1 hour.

Peptide cleavage was performed twice per resin following standard protocol in a solution of 95% TFA, 2.5% H2O, 2.5% TIS, and 20 mg/mL DTT for 1 hour at room temperature. The crude peptide was then precipitated in cold diethyl ether and subsequently lyophilized for 2 days. Completion of synthesis was confirmed by analyzing the samples using a Shimazu mass spectrometer and an HP 1100 analytical HPLC system before and after dye conjugation.

Ligand depletion sedimentation assay

The α-synuclein fibrils were diluted using the fibrillization solution and subsequently mixed with the peptide of interest. The final peptide concentration in each 400 µL sample was adjusted to 9.5 µM, while the concentrations of α-synuclein fibrils ranged from 5 to 40 µM. To create the

fibril-peptide solutions, each sample was composed of 0.17x of fibrillization solution and 0.36x PBS. For experimental replicates, 100 µL of each fibril-peptide solution was transferred to individual 1 mL non-stick Eppendorf tubes, which were then shaken at 400 rpm overnight at room temperature.

Following the incubation period, the samples were centrifuged at 2000 rpm for 20 minutes to pellet the fibrils. Subsequently, the supernatant was carefully collected and analyzed at the peak absorbance of FITC at 490 nm to measure the fluorescence signal associated with the presence of FITC-labeled peptide in the supernatant.

Confocal microscopy

Peptides were prepared by dissolving them in 1x PBS to various concentrations, including 128, 64, 32, 16, 8, 4, 2, and 1 nM. For the experimental setup, 50 µL aliquots of each peptide solution were dispensed into wells of a 384-well plate (Corning™ BioCoat™ 384-Well, Collagen Type I-Treated, Flat-Bottom Microplate). Subsequently, 1 µL of fibril solution was added to each well, achieving a final fibril concentration of 600 nM. Thorough mixing of the fibril and peptide solutions was achieved by pipetting up and down. To form pellets for imaging, the plate was then centrifuged at 50 x g.

Imaging of the fibril-peptide complexes was performed using a Leica SP8 confocal microscope equipped with a 40× water immersion lens (1.1 NA). The imaging utilized white light and 405 nm lasers, and fluorescence signals were detected using a HyD detector at 512 × 512-pixel resolution with a 0.75× zoom factor. Each field-of-view experiment was manually focused, ensuring a constant intensity of illumination. To minimize background noise originating from the

bottom of the well, the LightGate setting was adjusted to a range of 0.5 to 18 ns. Excitation and emission detection wavelengths were collected at 490/525 nm, 415/490 nm, and 561/594 nm for the imaging analysis.

References

(1) Nelson, R.; Sawaya, M. R.; Balbirnie, M.; Madsen, A. Ø.; Riekel, C.; Grothe, R.; Eisenberg, D. Structure of the Cross-Beta Spine of Amyloid-like Fibrils. *Nature* **2005**, *435* (7043), 773–778. https://doi.org/10.1038/nature03680.

(2) Fitzpatrick, A. W. P.; Debelouchina, G. T.; Bayro, M. J.; Clare, D. K.; Caporini, M. A.; Bajaj, V. S.; Jaroniec, C. P.; Wang, L.; Ladizhansky, V.; Müller, S. A.; MacPhee, C. E.; Waudby, C. A.; Mott, H. R.; De Simone, A.; Knowles, T. P. J.; Saibil, H. R.; Vendruscolo, M.; Orlova, E. V.; Griffin, R. G.; Dobson, C. M. Atomic Structure and Hierarchical Assembly of a Cross-β Amyloid Fibril. *Proc. Natl. Acad. Sci.* **2013**, *110* (14), 5468–5473. https://doi.org/10.1073/pnas.1219476110.

(3) Spillantini, M. G.; Crowther, R. A.; Jakes, R.; Hasegawa, M.; Goedert, M. Alpha-Synuclein in Filamentous Inclusions of Lewy Bodies from Parkinson's Disease and Dementia with Lewy Bodies. *Proc. Natl. Acad. Sci. U. S. A.* **1998**, *95* (11), 6469–6473. https://doi.org/10.1073/pnas.95.11.6469.

(4) Eisenberg, D.; Jucker, M. The Amyloid State of Proteins in Human Diseases. *Cell* **2012**, *148* (6), 1188–1203. https://doi.org/10.1016/j.cell.2012.02.022.

(5) Ke, P. C.; Zhou, R.; Serpell, L. C.; Riek, R.; Knowles, T. P. J.; Lashuel, H. A.; Gazit, E.; Hamley, I. W.; Davis, T. P.; Fändrich, M.; Otzen, D. E.; Chapman, M. R.; Dobson, C. M.; Eisenberg, D. S.; Mezzenga, R. Half a Century of Amyloids: Past, Present and Future. *Chem. Soc. Rev.* **2020**, *49* (15), 5473–5509. https://doi.org/10.1039/c9cs00199a.

(6) Tuttle, M. D.; Comellas, G.; Nieuwkoop, A. J.; Covell, D. J.; Berthold, D. A.; Kloepper, K. D.; Courtney, J. M.; Kim, J. K.; Barclay, A. M.; Kendall, A.; Wan, W.; Stubbs, G.; Schwieters, C. D.; Lee, V. M. Y.; George, J. M.; Rienstra, C. M. Solid-State NMR Structure of a Pathogenic

Fibril of Full-Length Human α-Synuclein. *Nat. Struct. Mol. Biol.* **2016**, *23* (5), 409–415. https://doi.org/10.1038/nsmb.3194.

(7) Diaz-Espinoza, R. Recent High-Resolution Structures of Amyloids Involved in Neurodegenerative Diseases. *Front. Aging Neurosci.* **2021**, *13*.

(8) Palladino, P.; Aura, A. M.; Spoto, G. Surface Plasmon Resonance for the Label-Free Detection of Alzheimer's β-Amyloid Peptide Aggregation. *Anal. Bioanal. Chem.* **2016**, *408* (3), 849–854. https://doi.org/10.1007/s00216-015-9172-6.

(9) Lövestam, S.; Koh, F. A.; van Knippenberg, B.; Kotecha, A.; Murzin, A. G.; Goedert, M.; Scheres, S. H. Assembly of Recombinant Tau into Filaments Identical to Those of Alzheimer's Disease and Chronic Traumatic Encephalopathy. *eLife* **2022**, *11*, e76494. https://doi.org/10.7554/eLife.76494.

(10) Close, W.; Neumann, M.; Schmidt, A.; Hora, M.; Annamalai, K.; Schmidt, M.; Reif, B.; Schmidt, V.; Grigorieff, N.; Fändrich, M. Physical Basis of Amyloid Fibril Polymorphism. *Nat. Commun.* **2018**, *9* (1), 699. https://doi.org/10.1038/s41467-018-03164-5.

(11) Emamzadeh, F. N. Alpha-Synuclein Structure, Functions, and Interactions. *J. Res. Med. Sci. Off. J. Isfahan Univ. Med. Sci.* **2016**, *21*, 29. https://doi.org/10.4103/1735-1995.181989.

(12) Murray, K. A.; Hu, C. J.; Griner, S. L.; Pan, H.; Bowler, J. T.; Abskharon, R.; Rosenberg, G. M.; Cheng, X.; Seidler, P. M.; Eisenberg, D. S. De Novo Designed Protein Inhibitors of Amyloid Aggregation and Seeding. *Proc. Natl. Acad. Sci. U. S. A.* **2022**, *119* (34), e2206240119. https://doi.org/10.1073/pnas.2206240119.

(13) Taş, K.; Volta, B. D.; Lindner, C.; El Bounkari, O.; Hille, K.; Tian, Y.; Puig-Bosch, X.; Ballmann, M.; Hornung, S.; Ortner, M.; Prem, S.; Meier, L.; Rammes, G.; Haslbeck, M.; Weber, C.; Megens, R. T. A.; Bernhagen, J.; Kapurniotu, A. Designed Peptides as

Nanomolar Cross-Amyloid Inhibitors Acting via Supramolecular Nanofiber Co-Assembly. *Nat. Commun.* **2022**, *13* (1), 5004. https://doi.org/10.1038/s41467-022-32688-0.

(14) Ladiwala, A. R. A.; Bhattacharya, M.; Perchiacca, J. M.; Cao, P.; Raleigh, D. P.; Abedini, A.; Schmidt, A. M.; Varkey, J.; Langen, R.; Tessier, P. M. Rational Design of Potent Domain Antibody Inhibitors of Amyloid Fibril Assembly. *Proc. Natl. Acad. Sci. U. S. A.* **2012**, *109* (49), 19965–19970. https://doi.org/10.1073/pnas.1208797109.

(15) Griner, S. L.; Seidler, P.; Bowler, J.; Murray, K. A.; Yang, T. P.; Sahay, S.; Sawaya, M. R.; Cascio, D.; Rodriguez, J. A.; Philipp, S.; Sosna, J.; Glabe, C. G.; Gonen, T.; Eisenberg, D. S. Structure-Based Inhibitors of Amyloid Beta Core Suggest a Common Interface with Tau. *eLife* **2019**, *8*, e46924. https://doi.org/10.7554/eLife.46924.

(16) Lu, J.; Cao, Q.; Wang, C.; Zheng, J.; Luo, F.; Xie, J.; Li, Y.; Ma, X.; He, L.; Eisenberg, D.; Nowick, J.; Jiang, L.; Li, D. Structure-Based Peptide Inhibitor Design of Amyloid-β Aggregation. *Front. Mol. Neurosci.* **2019**, *12*.

(17) Sievers, S. A.; Karanicolas, J.; Chang, H. W.; Zhao, A.; Jiang, L.; Zirafi, O.; Stevens, J. T.; Münch, J.; Baker, D.; Eisenberg, D. Structure-Based Design of Non-Natural Amino-Acid Inhibitors of Amyloid Fibril Formation. *Nature* **2011**, *475* (7354), 96–100. https://doi.org/10.1038/nature10154.

(18) Seidler, P. M.; Boyer, D. R.; Murray, K. A.; Yang, T. P.; Bentzel, M.; Sawaya, M. R.; Rosenberg, G.; Cascio, D.; Williams, C. K.; Newell, K. L.; Ghetti, B.; DeTure, M. A.; Dickson, D. W.; Vinters, H. V.; Eisenberg, D. S. Structure-Based Inhibitors Halt Prion-like Seeding by Alzheimer's Disease–and Tauopathy–Derived Brain Tissue Samples. *J. Biol. Chem.* **2019**, *294* (44), 16451–16464. https://doi.org/10.1074/jbc.RA119.009688.

(19) Plumley, J. A.; Ali-Torres, J.; Pohl, G.; Dannenberg, J. J. Capping Amyloid β-Sheets of the Tau-Amyloid Structure VQIVYK with Hexapeptides Designed To Arrest Growth. An ONIOM

and Density Functional Theory Study. *J. Phys. Chem. B* **2014**, *118* (12), 3326–3334. https://doi.org/10.1021/jp501890p.

(20) Henning-Knechtel, A.; Kumar, S.; Wallin, C.; Król, S.; Wärmländer, S. K. T. S.; Jarvet, J.; Esposito, G.; Kirmizialtin, S.; Gräslund, A.; Hamilton, A. D.; Magzoub, M. Designed Cell-Penetrating Peptide Inhibitors of Amyloid-Beta Aggregation and Cytotoxicity. *Cell Rep. Phys. Sci.* **2020**, *1* (2), 100014. https://doi.org/10.1016/j.xcrp.2020.100014.

(21) Sahtoe, D. D.; Andrzejewska, E. A.; Han, H. L.; Rennella, E.; Schneider, M. M.; Meisl, G.; Ahlrichs, M.; Decarreau, J.; Nguyen, H.; Kang, A.; Levine, P.; Lamb, M.; Li, X.; Bera, A. K.; Kay, L. E.; Knowles, T. P. J.; Baker, D. Design of Amyloidogenic Peptide Traps. bioRxiv January 13, 2023, p 2023.01.13.523785. https://doi.org/10.1101/2023.01.13.523785.

(22) Yang, H.; Yuan, P.; Wu, Y.; Shi, M.; Caro, C. D.; Tengeiji, A.; Yamanoi, S.; Inoue, M.; DeGrado, W. F.; Condello, C. EMBER Multidimensional Spectral Microscopy Enables Quantitative Determination of Disease- and Cell-Specific Amyloid Strains. *Proc. Natl. Acad. Sci.* **2023**, *120* (12), e2300769120. https://doi.org/10.1073/pnas.2300769120.

(23) Magnusson, K.; Simon, R.; Sjölander, D.; Sigurdson, C. J.; Hammarström, P.; Nilsson, K. P. R. Multimodal Fluorescence Microscopy of Prion Strain Specific PrP Deposits Stained by Thiophene-Based Amyloid Ligands. *Prion* **2014**, *8* (4), 319–329. https://doi.org/10.4161/pri.29239.

(24) Rasmussen, J.; Mahler, J.; Beschorner, N.; Kaeser, S. A.; Häsler, L. M.; Baumann, F.; Nyström, S.; Portelius, E.; Blennow, K.; Lashley, T.; Fox, N. C.; Sepulveda-Falla, D.; Glatzel, M.; Oblak, A. L.; Ghetti, B.; Nilsson, K. P. R.; Hammarström, P.; Staufenbiel, M.; Walker, L. C.; Jucker, M. Amyloid Polymorphisms Constitute Distinct Clouds of Conformational Variants in Different Etiological Subtypes of Alzheimer's Disease. *Proc.*

Natl. Acad. Sci. U. S. A. **2017**, *114* (49), 13018–13023. https://doi.org/10.1073/pnas.1713215114.

(25) Li, B.; Ge, P.; Murray, K. A.; Sheth, P.; Zhang, M.; Nair, G.; Sawaya, M. R.; Shin, W. S.; Boyer, D. R.; Ye, S.; Eisenberg, D. S.; Zhou, Z. H.; Jiang, L. Cryo-EM of Full-Length α-Synuclein Reveals Fibril Polymorphs with a Common Structural Kernel. *Nat. Commun.* **2018**, *9* (1), 3609. https://doi.org/10.1038/s41467-018-05971-2.

(26) Varadi, M.; De Baets, G.; Vranken, W. F.; Tompa, P.; Pancsa, R. AmyPro: A Database of Proteins with Validated Amyloidogenic Regions. *Nucleic Acids Res.* **2018**, *46* (D1), D387–D392. https://doi.org/10.1093/nar/gkx950.

(27) Mitternacht, S. FreeSASA: An Open Source C Library for Solvent Accessible Surface Area Calculations. *F1000Research* **2016**, *5*, 189. https://doi.org/10.12688/f1000research.7931.1.

(28) Zhou, J.; Grigoryan, G. Rapid Search for Tertiary Fragments Reveals Protein Sequence-Structure Relationships. *Protein Sci. Publ. Protein Soc.* **2015**, *24* (4), 508–524. https://doi.org/10.1002/pro.2610.

(29) Leman, J. K.; Weitzner, B. D.; Lewis, S. M.; Adolf-Bryfogle, J.; Alam, N.; Alford, R. F.; Aprahamian, M.; Baker, D.; Barlow, K. A.; Barth, P.; Basanta, B.; Bender, B. J.; Blacklock, K.; Bonet, J.; Boyken, S. E.; Bradley, P.; Bystroff, C.; Conway, P.; Cooper, S.; Correia, B. E.; Coventry, B.; Das, R.; De Jong, R. M.; DiMaio, F.; Dsilva, L.; Dunbrack, R.; Ford, A. S.; Frenz, B.; Fu, D. Y.; Geniesse, C.; Goldschmidt, L.; Gowthaman, R.; Gray, J. J.; Gront, D.; Guffy, S.; Horowitz, S.; Huang, P.-S.; Huber, T.; Jacobs, T. M.; Jeliazkov, J. R.; Johnson, D. K.; Kappel, K.; Karanicolas, J.; Khakzad, H.; Khar, K. R.; Khare, S. D.; Khatib, F.; Khramushin, A.; King, I. C.; Kleffner, R.; Koepnick, B.; Kortemme, T.; Kuenze, G.; Kuhlman, B.; Kuroda, D.; Labonte, J. W.; Lai, J. K.; Lapidoth, G.; Leaver-Fay, A.; Lindert, S.; Linsky,

T.; London, N.; Lubin, J. H.; Lyskov, S.; Maguire, J.; Malmström, L.; Marcos, E.; Marcu, O.; Marze, N. A.; Meiler, J.; Moretti, R.; Mulligan, V. K.; Nerli, S.; Norn, C.; Ó'Conchúir, S.; Ollikainen, N.; Ovchinnikov, S.; Pacella, M. S.; Pan, X.; Park, H.; Pavlovicz, R. E.; Pethe, M.; Pierce, B. G.; Pilla, K. B.; Raveh, B.; Renfrew, P. D.; Burman, S. S. R.; Rubenstein, A.; Sauer, M. F.; Scheck, A.; Schief, W.; Schueler-Furman, O.; Sedan, Y.; Sevy, A. M.; Sgourakis, N. G.; Shi, L.; Siegel, J. B.; Silva, D.-A.; Smith, S.; Song, Y.; Stein, A.; Szegedy, M.; Teets, F. D.; Thyme, S. B.; Wang, R. Y.-R.; Watkins, A.; Zimmerman, L.; Bonneau, R. Macromolecular Modeling and Design in Rosetta: Recent Methods and Frameworks. *Nat. Methods* **2020**, *17* (7), 665–680. https://doi.org/10.1038/s41592-020-0848-2.

(30) DiMaio, F.; Leaver-Fay, A.; Bradley, P.; Baker, D.; André, I. Modeling Symmetric Macromolecular Structures in Rosetta3. *PLOS ONE* **2011**, *6* (6), e20450. https://doi.org/10.1371/journal.pone.0020450.

(31) Maguire, J. B.; Boyken, S. E.; Baker, D.; Kuhlman, B. Rapid Sampling of Hydrogen Bond Networks for Computational Protein Design. *J. Chem. Theory Comput.* **2018**, *14* (5), 2751–2760. https://doi.org/10.1021/acs.jctc.8b00033.

(32) Boyer, D. R.; Li, B.; Sun, C.; Fan, W.; Zhou, K.; Hughes, M. P.; Sawaya, M. R.; Jiang, L.; Eisenberg, D. S. The α-Synuclein Hereditary Mutation E46K Unlocks a More Stable, Pathogenic Fibril Structure. *Proc. Natl. Acad. Sci. U. S. A.* **2020**, *117* (7), 3592–3602. https://doi.org/10.1073/pnas.1917914117.

(33) LeVine, H. Thioflavine T Interaction with Synthetic Alzheimer's Disease Beta-Amyloid Peptides: Detection of Amyloid Aggregation in Solution. *Protein Sci. Publ. Protein Soc.* **1993**, *2* (3), 404–410. https://doi.org/10.1002/pro.5560020312.

Publishing Agreement

It is the policy of the University to encourage open access and broad distribution of all theses, dissertations, and manuscripts. The Graduate Division will facilitate the distribution of UCSF theses, dissertations, and manuscripts to the UCSF Library for open access and distribution. UCSF will make such theses, dissertations, and manuscripts accessible to the public and will take reasonable steps to preserve these works in perpetuity.

I hereby grant the non-exclusive, perpetual right to The Regents of the University of California to reproduce, publicly display, distribute, preserve, and publish copies of my thesis, dissertation, or manuscript in any form or media, now existing or later derived, including access online for teaching, research, and public service purposes.

DocuSigned by:
Hailey Wallace
722C950175814C8...
Author Signature

8/28/2023
Date